Fault controls spatial variation of fracture density and rock mass strength within the Yarlung Tsangpo Fault damage zone (southern Tibet)

Xueliang Wang[1], Giovanni Battista Crosta[2], Doug Stead[3], Shengwen Qi[1], Paolo Frattini[4], Juanjuan Sun[1], and Haiyang Liu[1]

[1]Institute of Geology and Geophysics, Chinese Academy of Sciences
[2]Università degli studi di Milano Bicocca
[3]Simon Fraser University
[4]Universita' degli Studi di Milano - Bicocca

November 30, 2022

Abstract

Quantifying the relationship between faulting and the spatial geometrical and mechanical characteristics of a rock mass controlled by faulting is difficult, mainly because of varying lithology and rock mass characteristics, the effects of topography and vegetation and local erosion of weaker rock mass. In this study, the procedures, investigation approaches, evidence and criteria for defining the threshold distance for damage zones of Yarlung Tsangpo (YLTP) Fault of southern Tibet were studied quantitatively by combining the spatial variations of fracture density, rock mass strength, rockfall inventory and previous thermal evidence. The extent of threshold distance of damage zone of the YLTP Fault is estimated at 5.9±0.6km. The internal dynamic action of fault controls rock mass physical and mechanical properties in the study area. The fault first affects the characteristics of rock mass structures, and then the orientation of the rock structures influences the stability of slope leading to rockfall.

Fault controls spatial variation of fracture density and rock mass strength within the Yarlung Tsangpo Fault damage zone (southern Tibet)

Xueliang Wang[1,2*], Giovanni Battista Crosta[3*], Douglas Stead[4], Shengwen Qi[1,2], Paolo Frattini[3], Juanjuan Sun[1,2], Haiyang Liu[1,2]

[1]Key Laboratory of Shale Gas and Geoengineering, Institute of Geology and Geophysics, Chinese Academy of Sciences, Beijing 100029, China.

[2]Innovation Academy for Earth Sciences, CAS, Beijing 100029, China.

[3]Department of Earth and Environmental Sciences, Università degli Studi di Milano-Bicocca, Piazza della Scienza 4, Milano 20126, Italy.

[4]Department of Earth Sciences, Simon Fraser University, Burnaby, BC V5A 1S6, Canada.

Corresponding author: X.L. Wang (wangxueliang@mail.iggcas.ac.cn);
G.B. Crosta (giovannibattista.crosta@unimib.it).

Key Points:

- The extent of threshold distance of damage zone of the Yarlung Tsangpo Fault of southern Tibet is estimated at 5.9±0.6km.
- Both the fracture density and the cohesion of rock mass strength vary with the distance to the fault core showing power curve relations.
- Internal dynamic action of faults controls rock mass physical and mechanical properties in the study area.

Abstract

Quantifying the relationship between faulting and the spatial geometrical and mechanical characteristics of a rock mass controlled by faulting is difficult, mainly because of varying lithology and rock mass characteristics, the effects of topography and vegetation and local erosion of weaker rock mass. In this study, the procedures, investigation approaches, evidence and criteria for defining the threshold distance for damage zones of Yarlung Tsangpo (YLTP) Fault of southern Tibet were studied quantitatively by combining the spatial variations of fracture density, rock mass strength, rockfall inventory and previous thermal evidence. The extent of threshold distance of damage zone of the YLTP Fault is estimated at 5.9±0.6km. The internal dynamic action of fault controls rock mass physical and mechanical properties in the study area. The fault first affects the characteristics of rock mass structures, and then the orientation of the rock structures influences the stability of slope leading to rockfall.

Plain Language Summary

The extent of the fault damage zone remains an outstanding challenge confounding attempts to assess rock mass physical and mechanical properties, the effects on landscape evolution and slope stability, and to delineate safe places for human occupation and infrastructure development. Recent technological developments including Unmanned Aerial Vehicles, terrestrial laser scanning, photogrammetry and point cloud analysis software tools greatly enhance our ability to investigate the issues using the Yarlung Tsangpo Fault of southern Tibet as a case study where ideal geological conditions exist to investigate the relationship. The results have been compared with published data from the evidence of thermal effects related to the exactly same fault and show a good match between internal thermal action and rock mass physical and mechanical properties controlled by the same faulting.

1 Introduction

Faults and fault materials are a major controlling factor for superficial and shallow processes such as slope stability, groundwater flow and surface hydrology, underground excavations, hydrocarbons extraction and storage, and mining (De Joussineau & Aydin,2007; Bense et al., 2013; Laubach et al., 2014). Localized deformations at low confining stresses cause the formation of zones characterized by heterogeneous and anisotropic properties (Frankel et al., 2007; Gudmundsson, 2011). As a consequence, landslide susceptibility assessment (Wang et al., 2014), groundwater flow modeling (Faulkner et al., 2010; Bense et al., 2013) and design of superficial and underground structures (Aydin et al., 2004), require a detailed description of the zones affected by faulting (Faulkner et al., 2010). Fault core and damage zone are definitions which embrace the entire rock mass volume around a fault “plane” (Faulkner et al., 2010; Laubach et al., 2014). Such a volume can be affected by a more or less important deterioration due to the stress and displacement concentration. The fault core is the zone where most of the displacements are accommodated. The damage zone is the portion of rock mass characterized by secondary structures including mainly fractures, secondary faults and zones with more abundant micro-fracturing, porosity and groundwater flow. In landslide susceptibility mapping, the distance from fault core has been frequently used as an index to quantify the potential triggering of fault-related landslide (Wang et al.,2014). In general, the spatial extent of such a controlling factor is often defined empirically, or at a mesoscale with limited ground evidence and analysis of the type of fault and the local characteristics (Mizoguchi & K. Ueta, 2013). Consequently, we suggest this distance should be the main focus in the geological characterization of fault damage and its engineering importance.

In the geomorphological literature, it has been recognized that the geometrical and mechanical characteristics of a rock mass are both important in controlling relief and stability of slope (Burbank et al., 1996; Crosta et al., 2014; DiBiase et al., 2018). However, the fault-controlled spatial variation of geometrical characteristics (i.e. fracture density) and a quantitative description of the effects of faulting on the mechanical properties of the rocks within a specific threshold area have rarely been quantified (Caine et al., 1996; Faulkner et al., 2010; Laubach et al., 2014). Such quantification is often hampered by certain conditions mainly including: (1) large faults could result in varying rock mass characteristics within a specific area; (2) changes in lithology along and around the fault could render it difficult to have comparable conditions; (3) the effects of topography and vegetation obscuring damaged rock mass outcrops, limiting their number, size and distribution and then the possibility to build a robust data set; (4) the local erosion of sections of weaker rock mass. At the same time, some of the above listed features can support the characterization and analysis of these damaged zones, as by back analysis of landslides in areas with different landslide types and abundance. The availability of high-resolution topographic data (i.e. laser scanner and photogrammetric point clouds) can be of help at studying both small and large features supporting the description of the degree of fracturing at different spatial scales (Oskin et al., 2007).

As a consequence, in order to assess the susceptibility to landsliding of the rock mass strength for construction, it is important to define some basic rules for the identification, mapping, sampling and testing of the extent of these zones and the properties of the involved materials (e.g. breccias, cataclasite, mylonite). The total thickness of the fault zone will depend on the size of the fault, the total amount of cumulated displacement, the type of fault, the overburden depth for the considered zone of the fault, the affected lithology. Many of the same factors will also controls the physical, chemical and mechanical characteristics of the fault materials (Laubach et al., 2014). Using recent technologies including Unmanned Aerial Vehicle (UAV), terrestrial laser scanning, and photogrammetry and point cloud analysis software tools (e.g. AgiSoft, Photoscan and Coltop; Jaboyedoff et al.,2007), we attempted to determine the best procedures, investigation approaches, evidence and criteria for defining the threshold distance for damage zones around faults. Combining geometrical, mechanical characteristics and published thermal evidence (Quidelleur et al., 1997), quantitative description of the effects of faulting on rock mass physical and mechanical properties were quantified to reveal the dynamic action of fault.

2 Materials and Methods

In this study, we selected an area of Tibet where ideal geological conditions exist to investigate the relationship between faulting and the spatial geometrical and mechanical characteristics of a rock mass controlled by faulting (Figure 1). The area is affected by the Yarlung Tsangpo Fault that belongs to a south-dipping thrust system composed of at least five south dipping thrust faults (Heim & Gansser, 1939; Yin et al., 1999; Murphy & Yin, 2003). Yarlung Tsangpo suture zone between the Indian and the Eurasian plates has been reactivated by northward back thrusting and dextral strike-slip movement (Burg & Chen, 1984) with an underthrusting rate of 21.3 mm/yr of the Indian Shield (Murphy & Yin, 2003) and a right-lateral slip rate of 2.6±0.7 mm/yr (Chen et al., 2004). The nearly E–W trending suture zone extends for more than 2000 km in southern Tibet (Aitchison et al., 2011; Xu et al., 2015), whose deformation along the multiple fault planes of suture zone is complex and shows variations from place to place, depending mainly on its orientation (Yin et al., 1994; Xu et al., 2012). For the geological description of the area we relied on Quidelleur et al. (1997), Chen et al. (2004) and Xu et al. (2012,2015). The lithology of the area is mainly diorite and granite with a small component of gneiss.

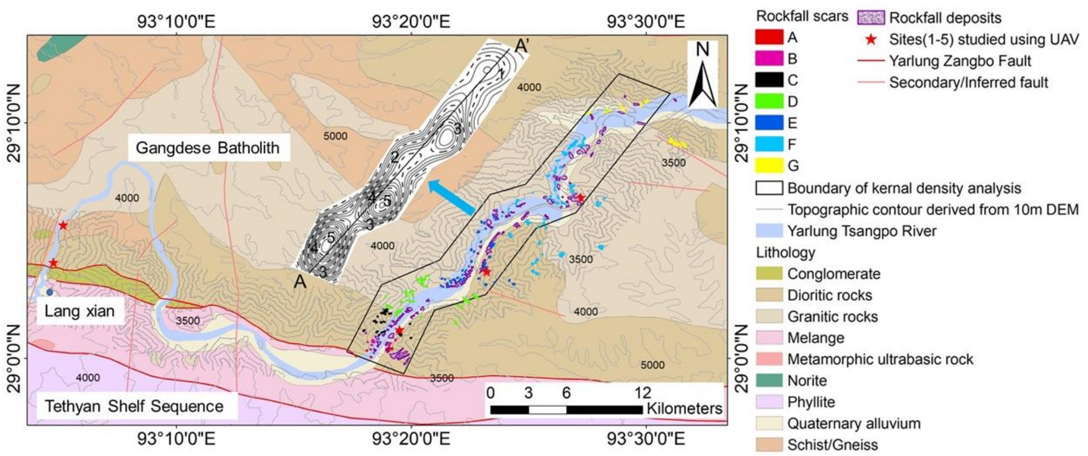

Figure 1. Location of the five surveying sites (1 to 5) and 360 rockfalls, including 237 rockfalls scars and 123 rockfalls deposits, with respect to the YLTP Fault core. Rockfall scars are zoned in 7 main clusters for back analysis of rock mass strength (Figure 4A), A to G, considering similar geometrical characteristics of the rock slopes and rock mass. Our 30-km measurement area covered by UAV at five sites and 10-m DEM for rockfalls identification on the whole slopes traverse along the Yarlung Tsangpo river valley. Rockfall iso-density contours obtained through bivariate kernel density estimation by ArcGIS are shown.

Both the geometrical characteristics of rock mass structures and rock mass strength could be controlled by a fault within a certain area (Osmundsen et al., 2009). The results of geometrical characteristics of rock mass structures and rock mass strength within the same fault zone should be consistent approximately if the approaches are used suitably. Hence, we firstly explored the spatial variation in the geometrical characteristics of the rock mass structures. Rock mass structures at the slope scale were identified and measured using a UAV at five selected sites at varied distances from the YLTP Fault core (Figure 1), with the consideration that exhumation doesn't influence fracture measurements at the surface (Savage & Brodsky, 2011). The selection of the sites was based on the outcrop rock mass conditions and the rock mass structures present. To get precise geometrical data of rock mass structures, we set at least six ground control points (GCP) at each site when flying Unmanned Aerial Vehicle (UAV). At each site, the same window was selected for measuring the dip/dip direction and spacing of all visible rock mass joints structures by PhotoScan (AgiSoft LLC, 2010), COLTOP (Jaboyedoff et al.,2007) and ArcMap.

Fracture density is an important parameter to quantify the character of the rock mass, which is used commonly in quantitative studies of damage zones (Faulkner et al., 2010). To estimate fracture density, we used three-dimensional (3D) geomechanical data to quantify joint volumetric count (Jv), with this taken as a measure of inter block size (ISRM, 1978) and of the total number of joints encountered in a cubic meter of fractured rock mass (Palmstrom, 2005; Messenzehl & Dikau, 2017). Meanwhile, to verify the data and results, we also measured independently the fallen block size using the UAV and Photoscan imagery.

Rock mass strength is a very difficult characteristics to be defined in a large area because of lack of suitable approaches and its inherent geology uncertainty (Hoek, 1983; Gudmundsson, 2011).Some studies (Hoek, 1994; Schmidt & Montgomery,1995 ; Evans et al., 1997;Shipton et al., 2002; Crosta et al., 2014) have tried to solve the problem. Various authors tackled the subject from a geomorphological and geomechanical point of view. Schmidt & Montgomery (1995) proposed an approach to define rock mass strength by analyzing relief and slope angle based on back analysis. Crosta et al. (2014) adopted an advanced geomechanical modeling approach to characterize rock masses on Mars starting from the distribution of landslides. Based on data of slope and relief of historical rockfall scars and reference to previous studies (Schmidt & Montgomery, 1995; Burbank et al., 1996; Montgomery & Brandon,2002; Crosta et al., 2014; DiBiase et al,2018), the rock mass strength of bedrock was back-calculated by the Culmann method under the precondition that bedrock relief is controlled by rock strength in the study area. When the present relief of bedrock areas is larger than the limit relief, the bedrock is prone to generate rockfalls. We located abundant scars left by rockfall on bedrock, and measured the relief at scar sites which were considered as limit relief thresholds. Then, the Culmann's two-dimensional slope stability model based on principles of limit-equilibrium was used to back-calculate the rock mass strength of the slope, which predicts a bounding relationship between hillslope gradient (β) and relief such that the maximum hillslope height (Hc) is given by (Culmann, 1875).

$$H_c = \frac{4C}{\rho g} \frac{sin\beta cos\varphi}{[1-\cos(\beta-\varphi)]} \quad (1)$$

where c is cohesion, and φ is the internal friction angle.

3 Results

The types of rock mass structures controlling the stability of slopes include pre-existing lithologic structures, tectonic and weathering structures (Stead & Wolter, 2015). For the granite rock mass exposed in the area and subjected to strong tectonism, the predominant structure type would be mainly due to tectonics and weathering (Townend et al., 2004). Overall a total of 2322 structures were measured including 537, 510, 560, 417 and 298 structures at sites 1 to 5 respectively (Figure 2). Based on the results, 5 predominant joint sets were identified in the study area. Joint sets J1 and J2, whose dips are greater than 56°, are conjugate joint sets created probably due to tectonism under a condition of vertical maximum principal stress. The two joint sets are most commonly and clearly exposed in the areas between sites 1 to 4. At site 5 and areas beyond that, joint sets J1 and J2 are few, with J1 absent in some places. Joint set J3 appears to represent unloading/stress-relief structures that parallel the slope surface and are exposed between sites 1 to 5. The dip of joint set J4 mainly exposed at sites 1 to 5 is less than 41°. Joint set J4 also represents unloading structures created during denudation of the diorites and granite. Joint set J5 whose mean dip is about 40° is mainly found at site 5 and areas beyond site 5. It should be noted that the dip/dip direction of the joint sets at the first four sites have very similar characteristics. In contrast, the dip/dip direction of the joints recorded at site 5 show significantly different characteristics including the disappearance of joint set, J1, and the appearance of joint set, J5 (Figure 3).

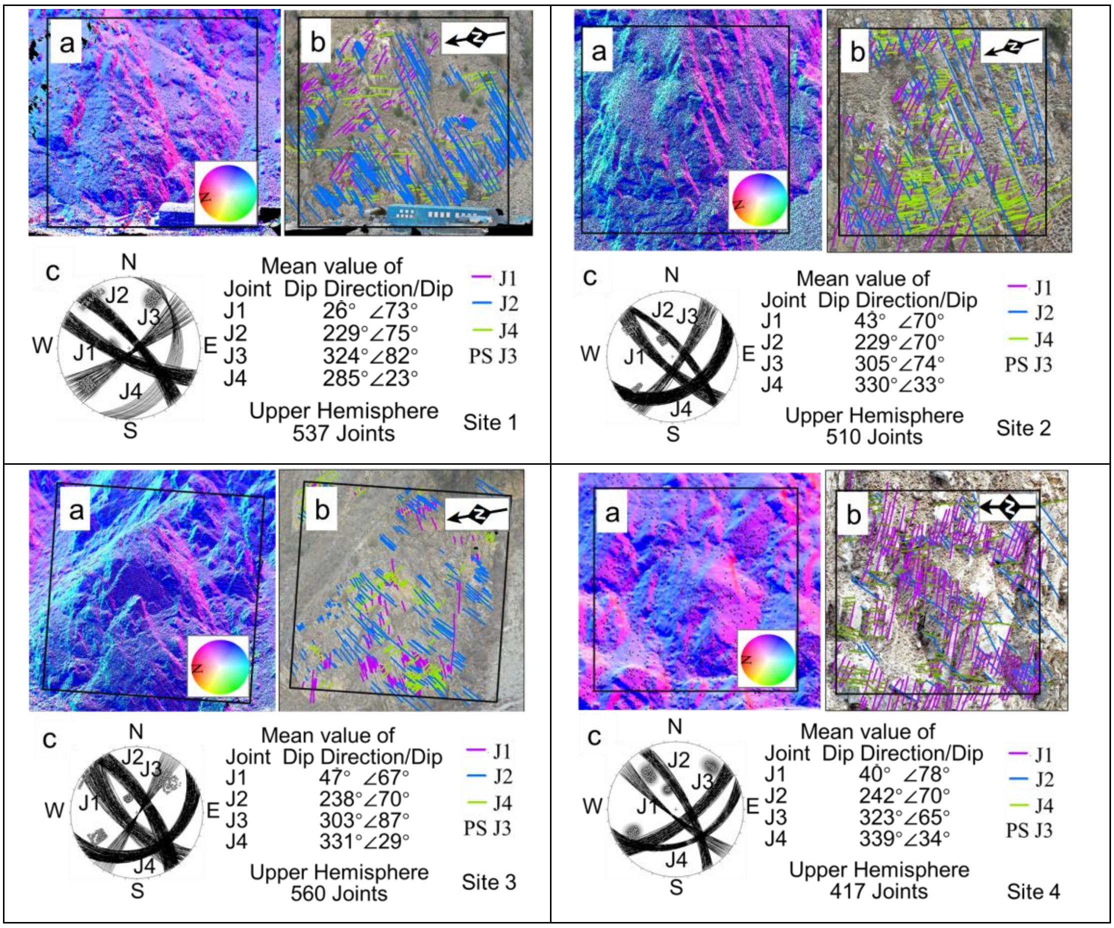

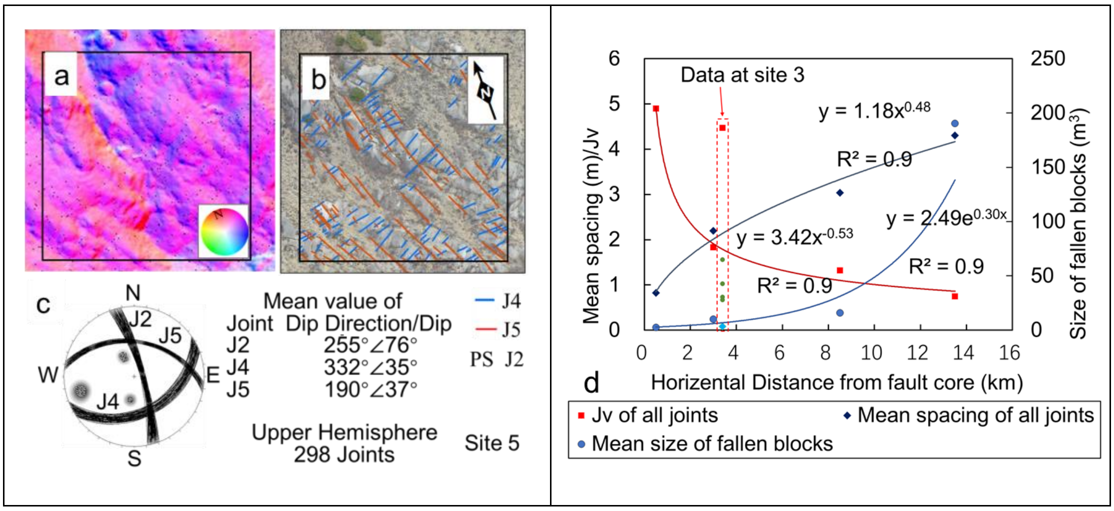

Figure 2. Coltop images (a) in colours representing the local orientation of five joint sets (b) at five sites (Figure 1 and Figure 3) and stereographic projections (c). At each site, a window of 100x100x100 m was selected for measuring the dip/dip direction (c) and spacing of all visible rock mass joints. The horizontal distances of the five sites from the YLZP Fault core are 0.5km, 3.0km, 3.4km, 8.5km and 13.5km (Figure 3). (d) Logarithmic and exponential relationships between mean spacing, computed Jv and fallen blocks' size with the distance from fault core.

The joint size measured is based on the quantity of data obtained by UAV, with a minimum joint spacing of 0.3m. The J1 to J4 joint set spacing is shown in Figure 2d based on the mean values to the distance from the fault core in damage zone. Influenced by tectonics, the relationship between mean spacing of joint sets with distance from the fault core show a strong power relationship with R^2 of 0.99 (Figure 2d). The rock mass exposed at site 3 in contrast to the other four sites is predominantly gneiss (Figure 1). The rock strength of the gneiss measured on site by Schmidt hammer testing (Aydin & Basu 2005) is lower than that of diorite and granite. As observed at site 3, the spacing of the joint sets within gneiss is smaller relative to the same joint sets in the diorite under the similar condition of tectonism (Figure 2d). For consistency here we only considered the spacing of the joint sets within the same diorite lithology.

The joint volumetric count, Jv, at varying distance (d) from the fault core is calculated using the joint set spacing and shows a strong power relationship (Jv=3.42×d^(-0.53)) with R^2 of 0.97 (Figure 2d). The bedrock rock mass strength (i.e. cohesion, c) varies with the distance (d) to the fault core showing a power curve relation (c=80.43×d^0.28) (Figure 3). A marked exponential distribution in the size of the fallen blocks with distance from the fault core is obtained with R^2 equals to 0.92 (Figure 2d). This indicated that the sizes of the rockfall blocks and the joint set spacing agree even when they are obtained by different methods.

Using data from helicopter-based remote sensing imagery and a DEM of 10 m resolution of the complete study area, a total of 360 historical rockfalls inventory including 237 rockfalls scars on bedrocks and 123 rockfalls deposits at toe of slopes were identified (Figure 1). Cohesion arises from the physical and chemical bonds in materials. The values of the cohesion calculated by the Culmann's approach show a significant increase with distance (Figure 3). The internal friction angle indicates the potential mobilized forces resisting motion along the failure plane. The values of internal friction angle show little fluctuation with the values from 23° to 28° at varied distances from fault core. The results may suggest that cohesion is an important component of hillslope-scale strength (Gallen et al., 2015).

4 Discussions

The results of the geometrical and mechanical analysis of the rock mass characteristics proved to be qualitatively consistent even when they were studied independently (Figure 3). Because of the influence of the fault, the rock mass strength values within a distance of 5.3km from the YLTP Fault core is less than 150kPa (Figure 3), which are close to the values in Longmenshan which are affected by the Beichuan fault and the Pengguan fault (Gallen et al., 2015), and are within the bounds of values estimated for hillslope-scale strength (Schmidt & Montgomery, 1995). The low values of rock mass strength in the area probably are the result of the characteristics of the fault damage zone. For the areas farther than 6.5 km from the fault core, the rock mass strength shows a significant increase (Figure 3). Using 360 rockfalls, we calculated the spatial variation of rockfall density obtained through bivariate kernel density estimation using ArcGIS (Figure 1). It can be also observed that the mean rockfall density within a distance of 6.5km the YLTP Fault is about three times the value obtained beyond this distance (Figure 3).

Combining the results, the extent of threshold distance of damage zone of the YLTP Fault is estimated at 5.9±0.6km. Quidelleur et al. (1997) studied internal thermal evolution related to thrusting using Biotite, K-feldspar and numerical simulation at the study area. A good match was observed between our threshold distance and the location of GR-18 that is the boundary in their thermal model (Figure 3). It presents a good evidence that evolution of physical, mechanical and thermal properties affected by fault in the study area is consistent.

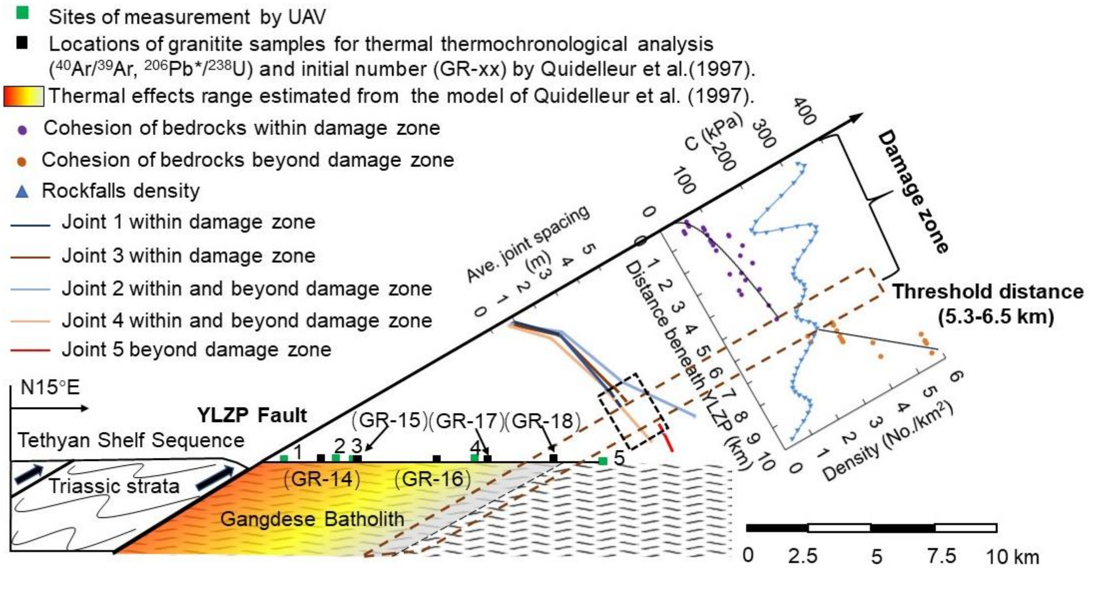

Figure 3. Extent of the damage zone of the thrust plane of the YLZP Fault. Considering

the divergency of 45° (Figure1) and a constant 30° dip to the south for the fault (Quidelleur et al.,1997), the five sites (1 to 5) are situated between 0 and 6.8 km from the hanging wall of the YLZP Fault. The exposure and average spacing of joint sets with the distance from fault core, using 2322 joints (Figure 2) measured by UAV at the five sites, are represented. Cohesion of bedrocks back calculated by means of the Culmann's approach on the whole slopes (Figure 4b) and the rockfall density extracted from Figure 1 along the A-A' profile vs distance from fault core are represented in the plots.

Previous studies indicated a trend of increasing damage zone width with displacement of fault, and that a lack of data for large faults (with displacements larger than 100 m) limits the possibility to find a statistically valid relationship for larger faults (Savage & Brodsky, 2011, De Joussineau & Aydin, 2007; Faulkner et al., 2010; Laubach et al., 2014; Torabi et al.,2019). Combining the displacement provided by Quidelleur et al. (1997) and our damage zone width, our result reaches values close to the maximum reported in literatures (Figure 4a).

Using the data of 237 historical outcropping rockfalls scars (Figure 1), a clear inverse relationship was observed between the mean slope angle and topographic relief (Figure 4b). This is similar to the results of Schmidt & Montgomery (1995), Crosta et al. (2014), Frattini & Crosta (2013) and DiBiase et al. (2018). Hence, we can also infer that the rock mass strength is a controlling factor on slope relief in the study area. However, Gabet et al. (2004) suggested that annual rainfall not rock mass strength is a controlling factor on relief in the whole Himalayas of central Nepal. In our selected study area in southern Tibet, the geological conditions are controlled by intense tectonic activity. The geometrical characteristics of rock mass structures (e.g. joint set dip/dip direction, joint set spacing, and joint volumetric count) show a significant spatial variation due to the influence of the cumulative displacement along the fault. The differences with respect to different scale and different geological settings (e.g. tectonically active sites) could be further studied in the future.

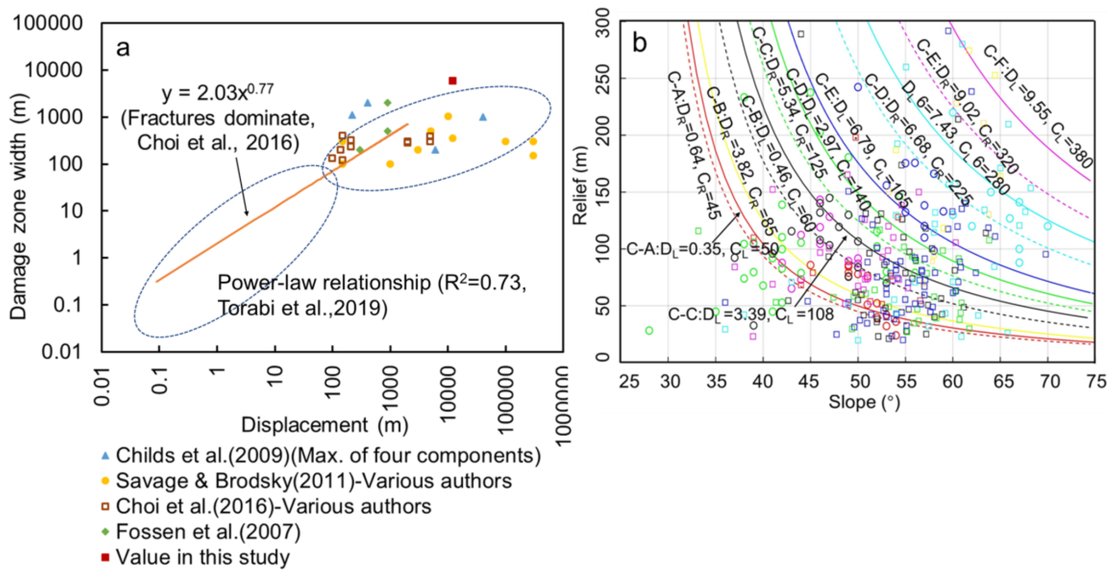

Figure 4. (a) Log–log plots of damage zone width against displacement of large faults

(>100 m displacement, Torabi et al., 2019) from the previous studies and our study on YLZP fault. (b) Relief vs slope angle at 237 rockfall scars (see Figure 1 for locations). Square and circle points represent data from left- (L)and right-hand (R) valley flanks. D_L and D_R (km) are the distances from fault core. C_L and C_R (kPa) are estimated cohesion values of bedrocks. C-A (to F) represent the 7 clusters (A to F) of rockfall scars in Figure 1.

Numerous studies (Khazai & Sitar,2004; Huang & Li, 2009; Qi et al,.2010) have noted that faults have an important influence on triggering landslides and rockfalls; some of these workers also discussed the relationships between number of landslides and distance from a fault. However, the process of faults controlling regional landsliding and rockfall still suffers from a lack of quantitative description. We quantitatively show that spatial variation of the rock mass strength shows different trend within and beyond the threshold distance due to the shift of geometrical characteristics of rock mass structures controlled by the YLZP Fault (Figure 3). Correspondingly, the density of rockfalls shows a significant shift at the threshold distance.

5 Conclusion

The extent of threshold distance of damage zone of the YLTP Fault is estimated at 5.9±0.6km, which reaches values close to the maximum reported in literatures. Within the threshold distance of YLTP Fault, both the joint volumetric count and the cohesion of rock mass strength vary with the distance to the fault core showing power curve relations.

Combining the studies, we concluded that internal dynamic action of faults controls rock mass physical and mechanical properties in the study area. To predict/assess the influence of faults in controlling regional landslide and rockfall distribution, the spatial variation of the geometrical characteristics of jointing is a key issue for future investigations.

Acknowledgments

This work was supported by the Strategic Priority Research Program of Chinese Academy of Sciences (Grant No. XDA23090402), Second Tibetan Plateau Scientific Expedition and Research Program (STEP) (Grant No. 2019QZKK0904), Application of Synthetic Aperture Radar-Based Geological Hazard Analysis Technology on the Strategic Electricity Transmission Passage of Sichuan-Tibet Plateau (Grant No. 52199918000C) and the Foundation of China Scholarship Council. The CARIPLO 2016-0756 @RockHoRiZon - Advanced Tools for Rockfall Hazard and Risk zonation at the regional scale Project is thanked. The authors wish to thank the program research group of State Grid Corporation of China for provision of the 10-m resolution topographic DEM data. All data used in this study are available at supporting information and Harvard Dataverse (that could be downloaded after logging in at this moment):

https://dataverse.harvard.edu/dataset.xhtml?persistentId=doi%3A10.7910%2FDVN%2FEWMHMU&version=DRAFT

References

Aitchison, J.C., Xia, X., Baxter, A.T., & Ali, J.R. (2011). Detrital zircon U–Pb ages along the Yarlung–Tsangpo suture zone, Tibet: implications for oblique convergence and collision between India and Asia. *Gondwana Research*, 20 (4), 691–709. https://doi.org/10.1016/j.gr.2011.04.002.

Aydin, A., Ozbek, A., & Cobanoglu, I. (2004). Tunneling in difficult ground: a case study from Dranaz tunnel, Sinop, Turkey. *Eng. Geol.*, 74(3-4), 293–301. https://doi.org/10.1016/j.enggeo.2004.04.003.

Aydin, A, & Basu, A. (2005). The Schmidt hammer in rock material characterization. *Eng. Geol.*, 81(1), 1-14. https://doi.org/10.1016/j.enggeo.2005.06.006

Bense, V.F., Gleeson, T., Loveless, S.E., Bour, O., & Scibek, J. (2013). Fault zone hydrogeology. *Earth Science Reviews*, 127, 171-192, http://dx.doi.org/10.1016/j.earscirev.2013.09.008.

Burbank, D.W., Leland, J., Fielding, E., Anderson, R.S., Brozovic, N., Reid, M.R., & Duncan, C. (1996). Bedrock incision, rock uplift and threshold hillslopes in the northwestern Himalayas. *Nature*, 379, 505-510. https://doi.org/10.1038/379505a0.

Burg, J.P., & Chen, G.M. (1984). Tectonics and structural zonation of southern Tibet, China. *Nature*, 311, 219–223. https://doi.org/10.1038/311219a0.

Caine, J.S., Evans, J.P., & Forster, C.B. (1996). Fault zone architecture and permeability structure. *Geology*, 24 (11), 1025-1028. https://doi.org/10.1130/ 0091-7613(1996)024<1025:FZAAPS>2.3.CO;2.

Chen Q., Freymueller J.T., Yang Z., Xu C.J., Jiang W.P., Wang Q., & Liu J.N. (2004). Spatially variable extension in southern Tibet based on GPS measurements. *Journal of Geophysical Research*, 109, B09401. https://doi.org/10.1029/2002JB002350.

Crosta, G.B., Utili, S., De Blasio, F.V., & Castellanza R. (2014). Reassessing rock mass properties and slope instability triggering conditions in Valles Marineris, Mars. *Earth and Planetary Science Letters*, 388, 329–342, https://doi.org/10.1016/j.epsl.2013.11.053.

Culmann, C. (1875). Die Graphische Statik: Zurich, Switzerland, Meyer and Zeller, 644 p.

De Joussineau, G., & Aydin, A. (2007). The evolution of the damage zone with fault growth in sandstone and its multiscale characteristics. *Journal of Geophysical Research*. 112, B12401. https://doi.org/10.1029/2006jb004711.

DiBiase, R.A., Rossi, M.W., & Neely, A.B. (2018). Fracture density and grain size controls on the relief structure of bedrock landscapes. *Geology*, 46(5), 399-402. https://doi.org/10.1130/g40006.1.

Evans, J.P., Forster, C.B., & Goddard, J.V. (1997). Permeability of fault-related rocks, and implications for hydraulic structure of fault zones. *J. Struct. Geol.*, 19 (11), 1393-1404. http://dx.doi.org/10.1016/S0191-8141(97)00057-6.

Faulkner, D.R., Jackson, C.A.L., Lunnc, R.J., Schlische, R.W., Shipton, Z.K., Wibberley, C.A.J., & Withjack, M.O. (2010). A review of recent developments concerning the structure, mechanics and fluid flow properties of fault zones: *J.*

Struct. Geol., 32(11), 1557-1575. https://doi.org/10.1016/j.jsg.2010.06.009.

Frankel, K. L., Dolan, J. F. Finkel, R. C. Owen, L. A. & Hoeft, J. S. (2007), Spatial variations in slip rate along the Death Valley-Fish Lake Valley fault system determined from LiDAR topographic data and cosmogenic 10Be geochronology, *Geophys. Res. Lett.*, 34, L18303, doi:10.1029/2007GL030549.

Frattini, P., & Crosta, G.B. (2013). The role of material properties and landsca pe morphology on landslide size distributions. *Earth and Planetary Science Letters*, 361, 310-319. https://doi.org/10.1016/j.epsl.2012.10.029.

Gallen S.F., Clark M.K., & Godt J.W. (2015). Coseismic landslides reveal near-surface rock strength in a high relief, tectonically active setting. *Geology*, 43(1), 11–14. https://doi.org/10.1130/g36080.1.

Gabet, E.J., Pratt-Sitaula, B.A., & Burbank, D.W. (2004). Climatic controls on hillslope angle and relief in the Himalayas. *Geology*, 32(7), 629–632. https://doi.org/10.1130/g20641.1.

Gudmundsson, A. (2011), Rock fractures in geological processes. New York, Cambridge University Press, 18p.

Heim, A., & Gansser, A. (1939). Central Himalaya, geological observations of the Swiss expeditions 1936. *Memoires de la Socie´te´ Helvetiques des Scie nces Naturelles*, 73, 1–245.

Hoek E. (1983). Strength of jointed rock masses, *Géotechnique*, 33(3), 187-223.

Hoek E. (1994). Strength of rock and rock masses, *ISRM News Journal*, 2(2), 4-16.

Huang, R., & Li, W. (2009). Analysis of the geo-hazards triggered by the 12 May 2008 Wenchuan Earthquake, China. *Bulletin of Engineering Geology and the Environment*, 68, 363–371. https://doi.org/10.1007/s10064-009-0207-0.

International Society for Rock Mechanics (ISRM), (1978). Commission on standardization of laboratory and field tests, Suggested methods for the quantitative description of discontinuities in rock masses. *Int. J. Rock Mech. Min. Sci. & Geomech. Abstr.*, 15(6), 319-368.

Jaboyedoff, M., Metzger, R., Oppikofer, T., Couture, R., Derron, M.H., Locat, J., & Turmel, D. (2007). New insight techniques to analyze rock-slope relief using DEM and 3D-imaging cloud points: COLTOP 3D software. *Proceedings of the 1st Canada-US rock mechanics Symposium*, Vancouver, Canada, 27–31 May 2007, https://doi.org/10.1201/NOE0415444019.

Khazai, B., & Sitar, N. (2004). Evaluation of factors controlling earthquake-induced landslides caused by Chi-Chi earthquake and comparison with the Northridge and Loma Prieta events. *Eng. Geol.*, 71(1-2), 79–95. https://doi.org/10.1016 /s0013-7952(03)00127-3.

Laubach, S.E., Eichhubl, P., Hargrove, P., Ellis, M.A., & Hooker, J.N. (2014). Fault core and damage zone fracture attributes vary along strike owing to interaction of fracture growth, quartz accumulation, and differing sandstone composition. *J. Struct. Geol*, 68 (part A), 207-226. https://doi.org/10.1016/j.jsg.2014.08.007.

Mizoguchi, K., & Ueta, K. (2013). Microfractures within the fault damage zone record the history of fault activity. *Geophys. Res. Lett.*, 40, 2023–2027, https://doi.org/10.1002/grl.50469

Messenzehl, K., & Dikau, R. (2017). Structural and thermal controls of rockfall frequency and magnitude within rockwall-talus systems (Swiss Alps). *Earth Surface Processes and Landforms*, 42(13), 1963–1981. https://doi.org/10.1002/esp.4155.

Montgomery, D.R., & Brandon, M.T. (2002). Topographic controls on erosion rates in tectonically active mountain ranges. *Earth and Planetary Science Letters*, 201(3-4), 481–489. https://doi.org/10.1016/s0012-821x(02)00725-2.

Murphy, M.A., & Yin, A. (2003). Structural evolution and sequence of thrusting in the Tethyan fold-thrust belt and Indus-Yalu suture zone, southwest Tibet. *Geological Society of America Bulletin*, 115(1), 21-34. https://doi.org/10.1130/0016-7606(2003)115<0021:SEASOT>2.0.CO;2

Oskin, M. E., Le, K. & Strane, M. D. (2007). Quantifying fault-zone activity in arid environments with highresolution topography. *Geophys. Res. Lett.*, 34, L23S05, https://doi.org/10.1029/2007GL031295

Osmundsen, P.T., Henderson, I., Lauknes, T.R., Larsen, Y., Redfield T.F., & Dehls J. (2009). Active normal fault control on landscape and rock-slope failure in northern Norway. *Geology*, 37(2), 135-138, https://doi.org/10.1130/g25208a.1.

Palmstrom, A. (2005). Measurements of and Correlations between Block Size and Rock Quality Designation (RQD). *Tunnels and Underground Space Technology*, 20(4), 362–377. https://doi.org/10.1016/j.tust. 2005.01.005

Qi S.W., Xu Q., Lan H.X., Zhang B. & Liu J.Y. (2010). Spatial distribution analysis of landslides triggered by 2008.5.12 Wenchuan Earthquake, China. *Eng. Geol.*, 116(1-2), 95-108. https://doi.org/10.1016/j.enggeo.2010.07.011.

Quidelleur X., Grove M., Lovera O.M., Harrison T. M., Yin A., & Ryerson F. J. (1997). Thermal evolution and slip history of the Renbu Zedong Thrust, southeastern Tibet. *Journal of Geophysical Research*, 102(B2), 2659-2679. https://doi.org/10.1029/96JB02483.

Shipton, Z.K., Evans, J.P., Robeson, K.R., Forster, C.B., & Snelgrove, S.S. (2002). Structural heterogeneity and permeability in faulted eolian sandstone: implications for subsurface modeling of faults. *AAPG Bull*. 86 (5), 863-883.

Savage H.M., & Brodsky E.E. (2011). Collateral damage: Evolution with displacement of fracture distribution and secondary fault strands in fault damage zones. *Journal of Geophysical Research*, 116, B03405. https://doi.org/10.1029/2010JB007665.

Schmidt, K.M., & Montgomery, D.R. (1995). Limits to relief. *Science*, 270(5236), 617-620. https://doi.org/ 10.1126/science.270.5236.617.

Stead, D., & Wolter, A. (2015). A critical review of rock slope failure mechanisms: The importance of structural geology. *J. Struct. Geol*, 74, 1-23. https://doi.org/10.1016/j.jsg.2015.02.002.

Torabi, A., Ellingsen, T.S.S., Johannessen, M.U., Alaei, B., Rotevatn, A. & Chiarella, D. (2019). Fault zone architecture and its scaling laws: where does the damage zone start and stop? *Geological Society*, London, Special Publications, 496, https://doi.org/10.1144/SP496-2018-151.

Townend, J., & M. D. Zoback (2004), Regional tectonic stress near the San Andreas fault in central and southern California. *Geophys. Res. Lett.*, 31, L15S11, https://doi.org/10.1029/2003GL018918

Wang, X.L., Zhang, L.Q., Wang, S.J., & Lari, S. (2014). Regional landslide susceptibility zoning with considering the aggregation of landslide points and the weights of factors. *Landslides*, 11, 399–409. https://doi.org/10.1007/s10346-013-0392-6.

Xu Z.Q, Ji S.C, Cai Z.H, Zeng L.S, Geng Q.R, & Cao H., (2012). Kinematics and dynamics of the Namche Barwa Syntaxis, eastern Himalaya: Constraints from deformation, fabrics and geochronology. *Gondwana Research*, 21(1), 19-36. https://doi.org/10.1016/j.gr.2011.06.010

Xu Z.Q, Dilek, Y., Yang, J.S., Liang, F.H., Liu, F., Ba, D.Z., Cai, Z.H., Li, G.W., Dong, H.W., & Ji, S.C. (2015). Crustal structure of the Indus–Tsangpo suture zone and its ophiolites in southern Tibet. *Gondwana Research*, 27(2), 507-524. https://doi.org/10.1016/j.gr.2014.08.001

Yin, A.,Harrison, T.M.,Ryerson, F.J.,Chen, W.,Kidd, W.S.F., & Copeland, P. (1994). Tertiary structural evolution of the Gangdese thrust system, southeastern Tibet. *Journal of Geophysical Research*, 99(B9), 18175–18201. https://doi.org/10.1029/94JB00504.

Yin, A., Harrison, T.M., Murphy, M.A., Grove, M., Nie, S., Ryerson, F.J., Wang, X., & Chen, Z. (1999). Tertiary deformation history in southeastern and southwestern Tibet during the Indo-Asian collision. *Geological Society of America Bulletin*, 111(11), 1644–1664. https://doi.org/10.1130/0016-7606(1999)111<1644:TDHOSA>2.3.CO;2